KINEMATIC DESIGN OF 3-RPSR PARALLEL MECHANISM FOR MOVABLE-DIE DRIVE MECHANISM OF PIPE BENDER

YUKIO TAKEDA[1], SATOSHI INADA[1], SHOHEI KAWASUMI[1], DAISUKE MATSUURA[1],
KAZUYA HIROSE[2], KEN ICHIRYU[2]

Abstract. The authors have been developing a pipe bender which fabricates pipes of three-dimensional complex shapes from straight pipes based on the penetration bending method. This bender is composed of a movable die supported by a drive mechanism, a fixed die and a pipe feeder. A 3-RPSR parallel mechanism was employed as the movable-die drive mechanism, and its kinematic design was figured out under the consideration of singularity and motion range of each joint to guarantee the capability for achieving a large orientation. Compliance characteristics and accuracy in pipe bending of the 3-RPSR mechanism taking into account the elastic deformation of links and servo compliances were discussed. A prototype pipe bender, which has been constructed based on the proposed kinematic design of the 3-RPSR mechanism, is shown. Experimental results of pipe bending using the prototype were shown and the effect of the improvement of orientation capability of the movable-die drive mechanism on the accuracy of bent pipe was discussed.

Key words: robotics, kinematics, statics, parallel mechanism, orientation capability, stiffness analysis, pipe bender.

1. INTRODUCTION

Three-dimensionally shaped products made of pipes or thin-plates (hereafter simply called as "pipe") having uniform cross-section along the longitudinal direction are popularly used as components in many applications, such as body frames of motor vehicles, handrails in buildings and components of welfare devices because of their contribution for mass reduction, rigidity improvement, cost reduction and fine appearance. Some products using bent pipes or thin-plates for assisting human motions are shown in Fig. 1. Since these products should be adaptable to each user of different physique, their components should be custom-made. Thus, machine tools for manufacturing such products should have flexibility in motion as well as rigidity of structure. Pipe bender based on the penetration bending method is one of the most effective solutions for such requirements. A configuration of pipe bender based on this method is shown in Fig. 2. The bender is

---

[1] Tokyo Institute of Technology, Department of Mechanical Sciences and Engineering, Japan
[2] Kikuchi Seisakusho Co., Ltd.

a   **b**

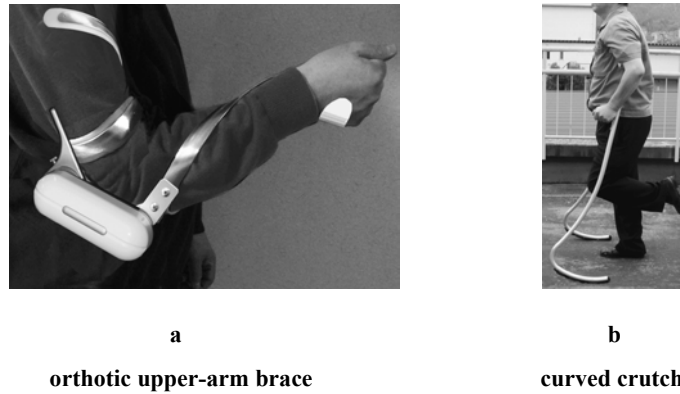**orthotic upper-arm brace**   **curved crutch**

Fig. 1 – Products using bent pipes or bent thin-plates for assisting human motions
(courtesy of Prof. Fujie in Waseda University and Kikuchi Seisakusho Co., Ltd.).
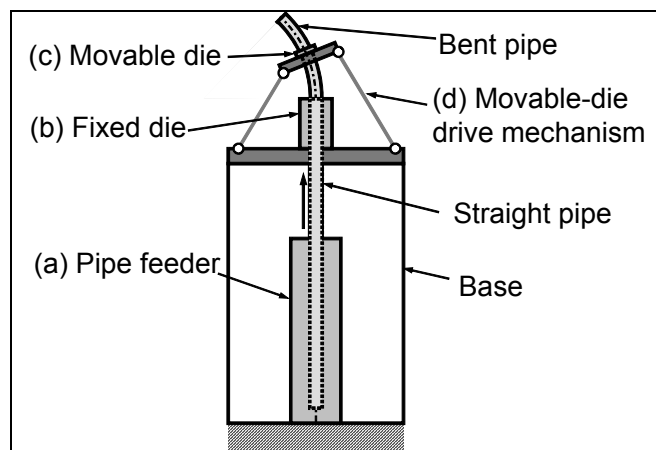

Fig. 2 – Configuration of pipe bender using penetration bending method.

basically composed of a movable die supported by a drive mechanism, a fixed die
and a pipe feeder. Based on the motion control of the movable die, the penetration
bending method makes it possible to bend a straight pipe of a constant cross-
section into a free spatial curve without changing tools or re-clamping of the pipe.
Since the position and orientation of the movable die at every moment should be
controlled in accordance with the target shape of the pipe, motions of the movable
die and the pipe feeder are synchronized each other. The cross-sections of the holes
of the dies should be identical with that of the external shape of the cross-section of
the pipe. By changing the dies according to the pipe, this method achieves bending
of pipes with an arbitrary cross-section. No expensive die with specified profile

corresponding to the desired curve of pipe is necessary. Moreover, adjustment of the bending can be easily done only by changing the motion of the movable die. This feature is quite advantageous in manufacturing custom-made devices and tools for improving their usability.

Penetration bending method has been proposed by Murata [1], and several pipe benders based on this method have been developed [2–7]. A determination method of the movable-die's motion based on Finite Element model has been developed [8]. To improve the accuracy of the bent pipe's shape, influence of the die geometry has been investigated [9], effects of steel grades and wall thickness on wrinkle formation, eccentricity, and ovality have been studied [10], and motion control software taking into account the springback properties has been developed [11]. It is known that the stretch bending [12] is a suitable way to reduce the wrinkling. Torque superposed spatial bending method has been developed for three-dimensional bending of profiles with symmetrical and asymmetrical cross-sections [13].

To simultaneously achieve high stiffness and motion flexibility of the movable-die drive mechanism, a spatial parallel mechanism with Stewart-Gough platform structure was applied [2, 3, 9]. However, improvement of orientation capability of the movable-die drive mechanism was demanded to achieve bending three-dimensional complex shaped pipes. Based on this background, we developed a pipe bender using a parallel mechanism with 3-RPSR structure having six degrees of freedom (DOF), which can achieve a good orientation capability [14], as the movable-die drive mechanism [15, 16]. Thanks to the special geometry of this mechanism such as the triple revolute joints located at the central axis on the base, and its structural and dimensional arrangement, this mechanism can perform a large output orientation capability such as an infinite rotation around the central axis and inclination by 45 deg in any direction. Through its application to pipe bending, we found that better orientation capability is required for manufacturing complex three-dimensional shaped pipes.

In the present paper, kinematic analysis of the 3-RPSR mechanism is performed to clarify the relationship between kinematic parameters and orientation capability taking into consideration the singularity and motion range of joints. Design of a prototype pipe bender based on the evaluation of orientation capability of this mechanism is presented. Compliance characteristics and position error of the movable die due to the compliance of the designed mechanism are investigated. Experimental results of pipe bending using the prototype bender are shown to investigate the effectiveness of the new design.

2. REQUIREMENTS FOR MOVABLE-DIE DRIVE MECHANISM

As shown in Fig. 2, a straight pipe is pressed upward by a pipe feeder and transformed into the desired shape in-between the fixed and movable dies. The

position and orientation of the movable die are controlled by the movable-die drive mechanism which is synchronized with the pipe feeding.

Let us consider a simple pipe-bending in $O_D - XZ$ plane as shown in Fig. 3a, in which the curvature of the pipe between the fixed and movable dies (within the area of θ in the figure) is constant. Z axis is identical to the pipe feeding axis. Given the curvature $\kappa = (1/R)$ (R – curvature radius), offset of the movable die (ξ_B, ζ_B), namely the coordinate of the center of the movable die P_B in $O_D - XZ$, are calculated using Eq. (1) for a specified θ.

$$\left.\begin{aligned} \xi_B &= R(1-\cos\theta) \\ \zeta_B &= R\sin\theta \end{aligned}\right\}. \tag{1}$$

Neglecting the friction between the pipe and dies, we obtain the following relationships among the pipe pushing force F_P, the force applied to the pipe by the movable die F_B, that by the fixed die F_C, and the bending moment of the pipe M on the basis of the force and moment equilibrium with respect to the pipe.

$$\left.\begin{aligned} F_C &= F_B\cos\theta \\ F_P &= F_B\sin\theta \\ M &= F_B\zeta_B\cos\theta + F_P\xi_B\sin\theta = F_B R\sin\theta \end{aligned}\right\}. \tag{2}$$

Equations (1) and (2) show that the larger angle θ contributes to the reduction in the magnitude of force on the dies, which leads to the reduction of

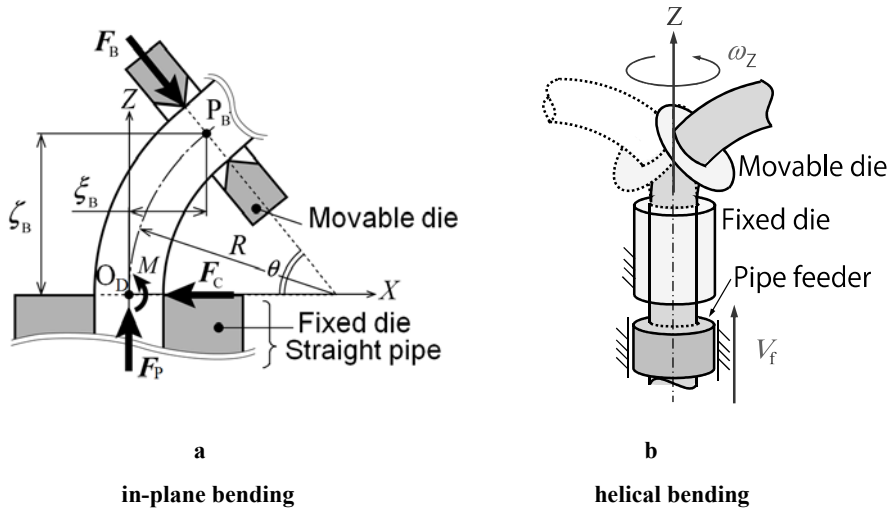a

in-plane bending

b

helical bending

Fig. 3 – Principle of penetration bending method.

energy consumption and improvement of accuracy of the bent pipe. It is also clear that the larger angle θ contributes to the easiness of interference avoidance among the components, such as the fixed and movable dies because the movable die can be offset more. Therefore, a large angle θ is required.

Let us consider another case for helical bending of a pipe. We consider a pipe with circular cross-section. A strategy to bend such pipe is shown in Fig. 3b. In this strategy, the movable die is rotated around Z axis at an angular velocity ω_Z, while the pipe is fed at a velocity V_f. By such a motion, direction of the pipe bending changes according to pipe feeding. As a result, torsion is given to the pipe, which results in bending a helical pipe. This strategy can be applied to bending pipes with a continuously changing curvature and torsion. In such a case, the movable-die drive mechanism is required to achieve a full rotation of the movable die around the pipe feeding axis while achieving a large angle θ.

Taking into account the bending strategies mentioned above, it is known that the movable-die drive mechanism is required to achieve a large angular motion range in θ, while achieving a full rotation around the pipe-feeding axis. To achieve a large angular displacement in θ and a full rotation around the pipe feeding axis while achieving a positioning of the movable die at any position, a 3-RPSR parallel mechanism with triple revolute joints on the base, which is shown in Fig. 4, is employed as the movable-die drive mechanism in our study. For easy bending of pipes with arbitrary cross-section, the movable-die drive mechanism is symmetrically located around the pipe feeding axis. The pipe feeding axis is identical to the vertical direction, which leads to a reduction of imbalanced application of gravitational force on the connecting chains of the movable-die drive mechanism.

As is known from the reference [7], there are a lot of machines for bending circular pipes in the market. Among them, 3-axis pipe benders are most popular and cost effective, and are one of the best solutions for bending pipes with circular cross-section. By using our solution using the 6-DOF parallel mechanism, manufacturing of pipes of complex three-dimensional shapes such as helical and twisted shapes with arbitrary cross-section as well as circular cross-section can be achieved.

As mentioned in Introduction, a 3-RPSR mechanism, which has already been synthesized and applied to our pipe bender, could not achieve bending well as the movable-die drive mechanism [15]. The major problems were insufficient orientation capability in θ and low stiffness. In the following sections of this paper, we discuss the design of the 3-RPSR mechanism with high orientation capability and effect of its compliance on the accuracy of the bent pipe.
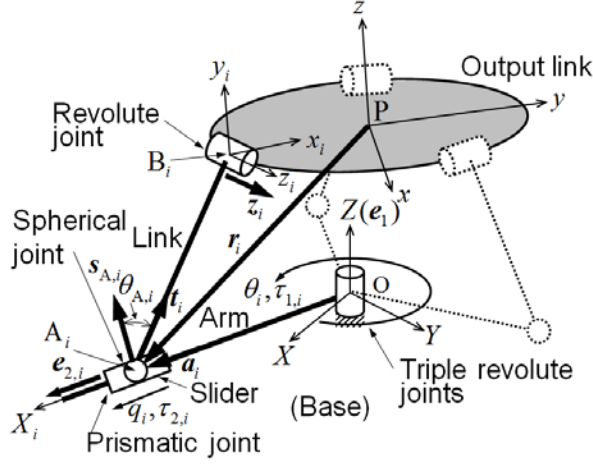
Fig. 4 – 3-RPSR mechanism with triple revolute joints.

3. KINEMATICS AND STATICS OF 3-RPSR MECHANISM

3.1. MECHANISM CONFIGURATION

The 3-RPSR mechanism shown in Fig. 4 is composed of three connecting chains with identical structure and dimensions. Each connecting chain is composed of revolute (R), prismatic (P), spherical (S) and revolute (R) joints arranged from the base to the output link. The axes of the revolute joints that connect the connecting chains with the base are coincident with the Z axis of the base coordinate frame O-XYZ. The three connecting chains are symmetrically located with respect to O-XYZ and the moving coordinate frame fixed on the output link P-xyz. P represents the reference point of the output link. The revolute joints on the base and the prismatic joints are active joints. As shown in Fig. 5, a moving coordinate frames B_i-$x_iy_iz_i$ and O_i-$X_iY_iZ_i$ are considered, while i represents the connecting chain number (i = 1, 2, 3). B_i-$x_iy_iz_i$ is fixed to the output link at point B_i, and direction of the z_i axis coincides with the axis of the revolute joint on the output link. O_i-$X_iY_iZ_i$ is fixed on the arm. The center of the spherical joint of i-th connecting chain is denoted as A_i. The orientation of the output link is represented by the three angles θ_y, θ_z, and ψ, shown in Fig. 6. Kinematic constants (Fig. 5) are r (radius of the location circle of the revolute joints on the output link), l (the link length $\overline{A_iB_i}$), and β_B (the angle between the axis of the prismatic joint and the base plane – XY plane).

In Fig. 4, $s_{A,i}$ is a unit vector heading the direction of the rotation center of the spherical joint. Swing angle of the spherical joint, $\theta_{A,i}$, is defined as the angle between $\overrightarrow{A_iB_i}$ and $s_{A,i}$. a_i and r_i represent the position vectors of A_i from the origin O and from the reference point P, respectively. t_i, e_1, $e_{2,i}$ and z_i are unit vectors representing the direction of the link $\overrightarrow{A_iB_i}$, that of the revolute joint on the base, that of the prismatic joint, and that of the rotation axis of the revolute joint at B_i, respectively.

Relationship among the three coordinate frames O-XYZ, P-xyz and B_i-$x_i y_i z_i$ is described based on 4×4 transformation matrices $T_{B,i}^P$, $T_{B,i}$ and T_P as following:

$$\begin{bmatrix} 1 \\ x \end{bmatrix} = T_P \begin{bmatrix} 1 \\ x^P \end{bmatrix} = T_P T_{B,i}^P \begin{bmatrix} 1 \\ x^{B,i} \end{bmatrix} = T_{B,i} \begin{bmatrix} 1 \\ x^{B,i} \end{bmatrix}, \tag{3}$$

where $T_{B,i} = \begin{bmatrix} 1 & 0\ 0\ 0 \\ B_i & R_{B,i} \end{bmatrix}$. x, x^P, $x^{B,i}$, $B_i = [X_{B,i}\ Y_{B,i}\ Z_{B,i}]^T$ and $R_{B,i} = [a_{mn}]$ ($m,n = 1,2,3$) are the position vectors written in O-XYZ, P-xyz and B_i-$x_i\ y_i\ z_i$ coordinate frames, and the position and orientation of the frame B_i-$x_i y_i z_i$ in terms of O-XYZ, respectively.

3.2. DISPLACEMENT ANALYSIS

First, we consider the inverse displacement analysis of the 3-RPSR mechanism. Point A_i moves on the surface of a circular cone defined by a point O, Z axis and angle β_B ($Z_{A,i} \le 0$). On the other hand, A_i lies on a circle of center B_i and radius l. These constraints are written by the following two equations and an inequality with respect to the coordinates of A_i (x_i, y_i, z_i) written in $B_i - x_i y_i z_i$.
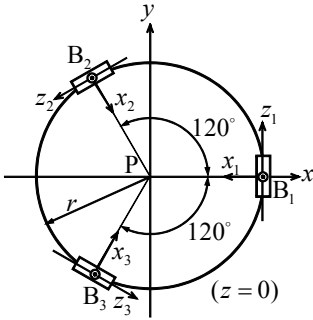

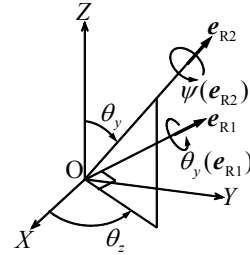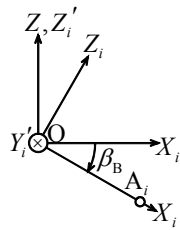Fig. 5 – Kinematic constants and location of revolute joints on output link.

Fig. 6 – Definition of orientation angles.

$$
\left.\begin{array}{l}
x_i^2 + y_i^2 = l^2 \\
\left\{(X_{\mathrm{B},i} + a_{11}x_i + a_{12}y_i)^2 + (Y_{\mathrm{B},i} + a_{21}x_i + a_{22}y_i)^2\right\}\tan^2 \beta_{\mathrm{B}} = (Z_{\mathrm{B},i} + a_{31}x_i + a_{32}y_i)^2 \\
Z_{\mathrm{B},i} + a_{31}x_i + a_{32}y_i \leq 0
\end{array}\right\} \qquad (4)
$$

By solving these simultaneous equations with an inequality, inverse displacement analysis is performed for a given T_{P} ($T_{\mathrm{B},i}$ is calculated from T_{P} and kinematic constants). Details of inverse displacement analysis including the discrimination of the working modes were discussed in [14].

Next, let us consider the forward displacement analysis. Consider the situation when all the input displacements are given. When all the active joints are fixed, the 3-RPSR mechanism becomes a 3-SR structure (mechanism with zero DOF) shown in Fig. 7a. This structure can be commonly seen by fixing the active joints of the 3–6 Stewart Platform mechanism with six SPS chains (Fig. 7b), the six-DOF parallel mechanism with three PPSR chains [17], and the three-DOF parallel mechanism with three SPR chains [18], while P stands for the active prismatic joint. As has been shown in [17], equations for the forward displacement analysis of the 3-SR structure result in a sixteenth-degree polynomial in one unknown. The equations can be derived based on the concept of the kinematic inversion from those of the 3-RS structure shown in Fig. 7c. The forward displacement analysis of the 3-RS structure has been discussed in [19–22] where the six-DOF parallel mechanism with three RPRS chains [19], the 6–3 Stewart Platform mechanism with six SPS chains [20], the six-DOF parallel mechanism with three PRPS chains [21] and the three-DOF mechanism with three RPS chains [22] were concretely considered. Therefore, the 3-RPSR mechanism has at most sixteen assembly modes.
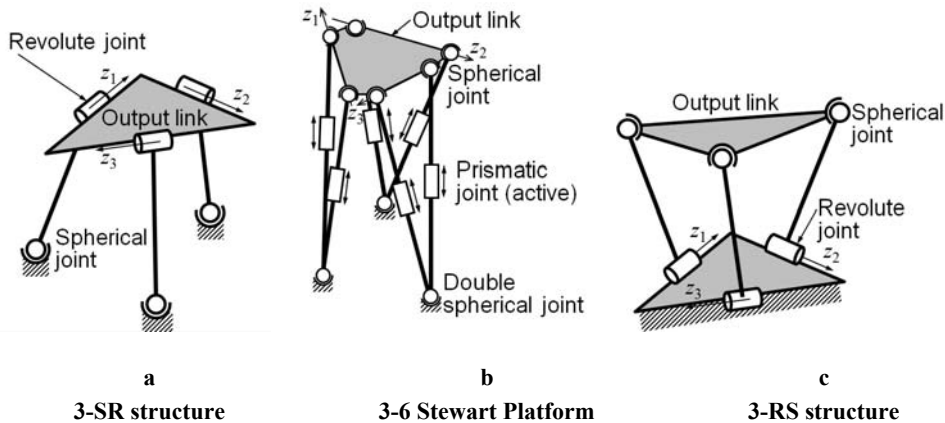

a	**b**	**c**
3-SR structure	**3-6 Stewart Platform**	**3-RS structure**

Fig. 7 – 3-SR structure, 3-6 Stewart Platform and 3-RS structure.

3.3. JACOBIAN MATRIX AND SINGULAR CONFIGURATION

According to the geometry of the connecting chain of the 3-RPSR mechanism, screws of the active joints $S_{1,i}$ (revolute joint) and $S_{2,i}$ (prismatic joint) of i-th connecting chain are described as

$$S_{1,i} = \begin{bmatrix} e_1 \\ e_1 \times (a_i - r_i) \end{bmatrix}, S_{2,i} = \begin{bmatrix} 0 \\ e_{2,i} \end{bmatrix}, \tag{5}$$

where these screws are written with respect to P as the reference point. The screws, $S_{R1,i}$ and $S_{R2,i}$, which are reciprocal to all the passive joint screws of i-th connecting chain, are written as follows

$$S_{R1,i} = \begin{bmatrix} t_i \\ r_i \times t_i \end{bmatrix}, S_{R2,i} = \begin{bmatrix} z_i \\ r_i \times z_i \end{bmatrix}. \tag{6}$$

Then, relationship between the input velocity $\dot{q} = [\dot{\theta}_1 \quad \dot{\theta}_2 \quad \dot{\theta}_3 \quad \dot{q}_1 \quad \dot{q}_2 \quad \dot{q}_3]^{\mathrm{T}}$ and the output velocity $V = [v_X \quad v_Y \quad v_Z \quad \omega_X \quad \omega_Y \quad \omega_Z]^{\mathrm{T}}$, where $\dot{\theta}_i$ and $\dot{q}_i$ are velocities of the active revolute and prismatic joints of i-th connecting chain, and v_j and ω_j $(j = X, Y, Z)$ are velocity of P in j-direction and angular velocity around j-axis of the output link, is written as

$$J_1^{\mathrm{T}} V = J_2^{\mathrm{T}} \dot{q}, \tag{7}$$

where $J_1 = \begin{bmatrix} t_1 & t_2 & t_3 & z_1 & z_2 & z_3 \\ r_1 \times t_1 & r_2 \times t_2 & r_3 \times t_3 & r_1 \times z_1 & r_2 \times z_2 & r_3 \times z_3 \end{bmatrix}$,

and

$$J_2 = \begin{bmatrix} \{a_1 \times t_1, e_1\} & 0 & 0 & \{a_1 \times z_1, e_1\} & 0 & 0 \\ 0 & \{a_2 \times t_2, e_1\} & 0 & 0 & \{a_2 \times z_2, e_1\} & 0 \\ 0 & 0 & \{a_3 \times t_3, e_1\} & 0 & 0 & \{a_3 \times z_3, e_1\} \\ \{t_1, e_{2,1}\} & 0 & 0 & \{z_1, e_{2,1}\} & 0 & 0 \\ 0 & \{t_2, e_{2,2}\} & 0 & 0 & \{z_2, e_{2,2}\} & 0 \\ 0 & 0 & \{t_3, e_{2,3}\} & 0 & 0 & \{z_3, e_{2,3}\} \end{bmatrix}.$$

Using this equation, relationship between the force F/ moment M exerted at P on the output link and driving force/moment of the active joints τ is written as

$$\begin{bmatrix} \boldsymbol{F} \\ \boldsymbol{M} \end{bmatrix} = -J^{\mathrm{T}} \boldsymbol{\tau} \,, \ J^{\mathrm{T}} = J_1 J_2^{-1} \,, \tag{8}$$

where $\boldsymbol{\tau} = \begin{bmatrix} \tau_{1,1} & \tau_{1,2} & \tau_{1,3} & \tau_{2,1} & \tau_{2,2} & \tau_{2,3} \end{bmatrix}^{\mathrm{T}}$. $\tau_{1,i}$ denotes the driving torque of the revolute joint on the base, and $\tau_{2,i}$ denotes the driving force of the prismatic joint of i-th connecting chain, respectively. J is the Jacobian matrix including closed-loop constraint.

Singular configurations of mechanisms are classified [23–25] into: (a) uncertain configuration, (b) stationary configuration, (c) combined configuration of (a) and (b), and (d) configuration with local mobility. Singular configurations of parallel mechanisms have been investigated in terms of the velocity relationship between the input and the output [21, 26], the force equation [27], the closure equation for the velocity of the mechanism [28], simple geometrical rules [29], the pressure angle [30], and so forth. We investigate the uncertain and stationary configurations of the 3-RPSR mechanism using the matrices J_1, J_2 and J in Eqs. (7) and (8) based on the velocity relationship between the input and the output. When the rank of the matrix J in Eq. (8) is deficient, the mechanism is located at a singular configuration. We can check the positions (loci) of singular configurations by the determinants of these matrices (zero or infinity). Singular configurations of the mechanism are classified as follows.

a) Uncertain configuration. At this configuration, the matrix J_1 loses its full rank. Typical configurations are: (a-1) axes of revolute joints on the output link z_i and points A_i of two connecting chains are located in a plane, (a-2) points A_i of two connecting chains coincide. The case (a-2) is not physically available due to the collision of two arms. Example of (a-1) is shown in Fig. 8a.

b) Stationary configuration. At this configuration, the matrix J_2 loses its rank. This configuration occurs when Eq. (4) in one connecting chain has a multiple root. Example of this singular configuration is shown in Fig. 8b.

a
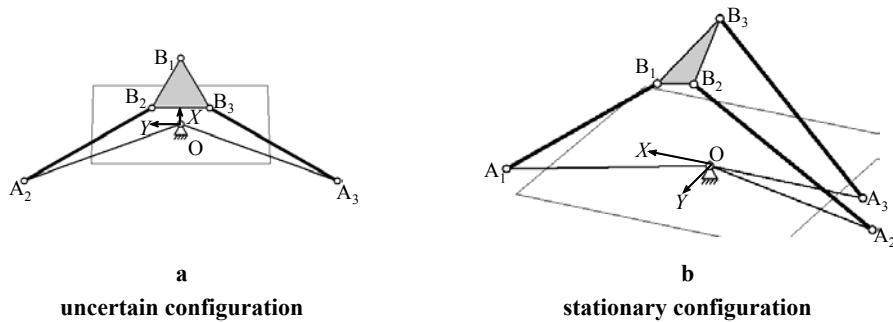**uncertain configuration**

b
stationary configuration

Fig. 8 – Example of singular configurations.

Similar to the case of the forward displacement analysis, the singular configuration of this mechanism is theoretically equivalent to those of the mechanisms mentioned in the previous subsection.

As well as the singular configurations mentioned above, motion range of the spherical joint at A_i is one of the predominant factors of the orientation capability because motion range of practical spherical joints is quite limited. In the next section, orientation capability of the 3-RPSR mechanism is investigated taking into consideration these factors.

3.4. COMPLIANCE ANALYSIS

We consider the output pose error caused by the external load exerted on the output link for pipe bending. This error is characterized by the compliance of the mechanism, which comes from the elastic deformations of the components of the mechanism such as links, bearings, reduction gears and ball screws, and the stiffness in servo controller. Compliance characteristics of the mechanism may include nonlinearity caused by contact deformations in bearings, large deformations of components under large load condition and buckling in joints [31]. In the present paper, we investigate the compliance characteristics of the mechanism using the linear model. There are three approaches for compliance analysis of mechanisms: (a) finite element analysis, (b) structural matrix analysis, and (c) virtual joint method. Though the approaches (a) and (b) provide better accuracy, they need high computational costs and detailed structural model of components. So, they are appropriate for the final design stage of mechanisms, however, they are not useful for compliance characterization. We use the virtual joint method for compliance analysis of the 3-RPSR mechanism. There are several modeling methods of compliance in parallel mechanisms. The compliance of actuators in parallel mechanism was considered in [32], compliance of the links as well as the actuators was considered in [33], detailed compliance characteristics of passive chains were considered in [34], kinetostatic model of compliant parallel mechanism based on the kinematic constraints and static equilibrium between the joint displacements and external loads was developed in [35], modeling method of stiffness of manipulators with passive joints taking into consideration the external loading condition was developed in [31]. We investigate the compliance characteristics of the 3-RPSR mechanism based on the virtual joint method taking into account the following elastic deformations of links and servo compliances as the elastic sources:

(L-1) Elastic deformation of the link A_iB_i in the longitudinal direction caused by the force, applied at A_i in the direction of $\overrightarrow{A_iB_i}$, $f_{L1,i}$ (Fig. 9);

(L-2) Elastic deformation of the link A_iB_i in the lateral direction caused by the force, applied at A_i in the direction of z_i, $f_{L2,i}$ (Fig. 9);
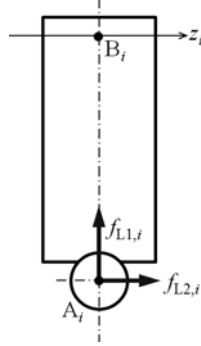
Fig. 9 – Forces applied to link A_iB_i.

(S-1) Displacement of the active revolute joint caused by its servo compliance;

(S-2) Displacement of the active prismatic joint caused by its servo compliance.

Following the virtual joint approach for stiffness/compliance analysis of mechanisms [33], relationship between the virtual actuation forces $\boldsymbol{f}_{L1} = [f_{L1,1} \quad f_{L1,2} \quad f_{L1,3}]^T$, $\boldsymbol{f}_{L2} = [f_{L2,1} \quad f_{L2,2} \quad f_{L2,3}]^T$ and the external force $[\boldsymbol{F}^T \quad \boldsymbol{M}^T]^T$ is described using the matrix J_1 in Eq. (7) as

$$\begin{bmatrix} \boldsymbol{F} \\ \boldsymbol{M} \end{bmatrix} = -J_1 \begin{bmatrix} \boldsymbol{f}_{L1} \\ \boldsymbol{f}_{L2} \end{bmatrix}. \tag{9}$$

Deformations/displacements of the links and servo systems corresponding to the forces $\boldsymbol{f}_{L1}$ and $\boldsymbol{f}_{L2}$ and the actuation forces/torques $\boldsymbol{\tau}_{S1} = [\tau_{1,1} \quad \tau_{1,2} \quad \tau_{1,3}]^T$ and $\boldsymbol{\tau}_{S2} = [\tau_{2,1} \quad \tau_{2,2} \quad \tau_{2,3}]^T$ are denoted as $\Delta\boldsymbol{x}_{L1}$, $\Delta\boldsymbol{x}_{L2}$, $\Delta\boldsymbol{x}_{S1}$ and $\Delta\boldsymbol{x}_{S2}$, respectively. The total displacement of the output link $[\Delta\boldsymbol{X}^T \quad \Delta\boldsymbol{\Theta}^T]^T$ ($\Delta\boldsymbol{X}$: displacement of point P, $\Delta\boldsymbol{\Theta}$: rotational displacement) caused by these deformations/displacements is written using the matrices J_1 and J as

$$\begin{bmatrix} \Delta\boldsymbol{X} \\ \Delta\boldsymbol{\Theta} \end{bmatrix} = \left(J_1^T\right)^{-1} \begin{bmatrix} \Delta\boldsymbol{x}_{L1} \\ \Delta\boldsymbol{x}_{L2} \end{bmatrix} + \left(J^T\right)^{-1} \begin{bmatrix} \Delta\boldsymbol{x}_{S1} \\ \Delta\boldsymbol{x}_{S2} \end{bmatrix}, \tag{10}$$

assuming small displacements. Assuming that the relationship between the deformation/displacement and the force/moment in each elastic source is linear, the following relationships hold:

$$\begin{bmatrix} \Delta\boldsymbol{x}_{L1} \\ \Delta\boldsymbol{x}_{L2} \end{bmatrix} = -C_L \begin{bmatrix} \boldsymbol{f}_{L1} \\ \boldsymbol{f}_{L2} \end{bmatrix}, \quad C_L = \begin{bmatrix} \mathrm{diag}[1/k_{L1}]_{3\times3} & 0_{3\times3} \\ 0_{3\times3} & \mathrm{diag}[1/k_{L2}]_{3\times3} \end{bmatrix}, \tag{11}$$

$$\begin{bmatrix} \Delta \boldsymbol{x}_{\mathrm{S1}} \\ \Delta \boldsymbol{x}_{\mathrm{S2}} \end{bmatrix} = -C_{\mathrm{S}} \begin{bmatrix} \boldsymbol{\tau}_{\mathrm{S1}} \\ \boldsymbol{\tau}_{\mathrm{S2}} \end{bmatrix}, \quad C_{\mathrm{S}} = \begin{bmatrix} \mathrm{diag}[1/k_{\mathrm{S1}}]_{3\times3} & 0_{3\times3} \\ 0_{3\times3} & \mathrm{diag}[1/k_{\mathrm{S2}}]_{3\times3} \end{bmatrix}, \quad (12)$$

where matrices C_{L} and C_{S} are the diagonal compliance matrices of the links and the servo systems, and k_{L1}, k_{L2}, k_{S1} and k_{S2} are corresponding coefficients, respectively. Using Eqs. (9)–(12), the following relationship between the external force and the displacement of the output link is obtained.

$$\begin{aligned} \begin{bmatrix} \Delta X \\ \Delta \boldsymbol{\Theta} \end{bmatrix} &= \left(J_1^{\mathrm{T}} \right)^{-1} \begin{bmatrix} \Delta \boldsymbol{x}_{\mathrm{L1}} \\ \Delta \boldsymbol{x}_{\mathrm{L2}} \end{bmatrix} + \left(J^{\mathrm{T}} \right)^{-1} \begin{bmatrix} \Delta \boldsymbol{x}_{\mathrm{S1}} \\ \Delta \boldsymbol{x}_{\mathrm{S2}} \end{bmatrix} \\ &= \left\{ \left(J_1^{\mathrm{T}} \right)^{-1} C_{\mathrm{L}} J_1^{-1} + \left(J^{\mathrm{T}} \right)^{-1} C_{\mathrm{S}} J^{-1} \right\} \begin{bmatrix} F \\ M \end{bmatrix} \\ &= \left(C_{\mathrm{ML}} + C_{\mathrm{MS}} \right) \begin{bmatrix} F \\ M \end{bmatrix} \\ &= C_{\mathrm{MT}} \begin{bmatrix} F \\ M \end{bmatrix} \end{aligned} \qquad (13)$$

The matrices C_{ML} and C_{MS} are the compliance matrices of the mechanism corresponding to the elastic deformation of the links and the servo compliances, respectively, and C_{MT} is the total compliance matrix of the mechanism.

4. ANALYSIS OF ORIENTATION CAPABILITY AND KINEMATIC DESIGN OF 3-RPSR MECHANISM

4.1. EVALUATION INDICES

Taking into consideration a typically required movement of a movable-die drive mechanism in bending a helical pipe, the target output motion used in the design of the mechanism was given as

$$\left. \begin{aligned} & X_{\mathrm{P}} = X'' \cos\theta_z, \, Y_{\mathrm{P}} = X'' \sin\theta_z, \, Z_{\mathrm{P}} = Z_{\mathrm{D}} + \left| \frac{S_Z}{S_X} X'' \right|, \theta_y = \frac{\theta_{y,\max}}{S_X} X'', \\ & \psi = 0, \theta_z = (i-1)\pi/9 (i = 1, \cdots, 6), \, X'' : [-S_X, S_X] \end{aligned} \right\}. \qquad (14)$$

Here, S_X and S_Z are the maximum strokes of P_B in the XY plane and in Z direction, and $\theta_{y,\max}$ is the maximum inclination angle of the movable die.

As an example of results, changes of det J and the swing angle of the spherical joint max$(\theta_{A,i})_{i=1,2,3}$ (denoted as $\theta_{A,max}$) with respect to orientation angle θ_y for a mechanism of $r=45$ mm, $l=150$ mm, $\beta_B=0$ deg are shown in Fig. 10 for $S_X=S_Z=16$ mm, $\theta_{y,max}=90$ deg. In our study, we consider a case of bending a pipe of diameter $D=8$ mm into the target curvature radius $R/D \geq 2$. The condition $R/D=2$ is considered to be the allowable limit of bending in the theory of plasticity. At a pose $X_P=Y_P=0$, $Z_P=Z_D$, $\theta_y=\theta_z=\psi=0$, the direction of swing center of the spherical joint $s_{A,i}$ was determined where Z_D was given such that orientation capability would be optimal. From Fig. 10, we found the following results.

(1) Maximum inclination angle, $\max(|\theta_y|)$, depends on the direction (θ_z).

(2) Swing angle of spherical joint $\theta_{A,max}$ linearly changes according to θ_y.

In the application of the mechanism to the movable-die drive mechanism, both the maximum of the maximum inclination angles at a constant θ_z, denoted as max$(\theta_{y,1}(\theta_z=$const.$))$, and the minimum of the maximum inclination angle at a constant θ_z, denoted as min$(\theta_{y,2}(\theta_z=$const.$))$, are important, where $\theta_{y,1}(\theta_z=$const.$)$ and $\theta_{y,2}(\theta_z=$const.$)$ are shown in the figure. As for the requirement to the spherical joint, smaller value of the ratio of the maximum swing angle $\theta_{A,max}$ at max$(\theta_{y,1}(\theta_z=$const.$))$ to max$(\theta_{y,1}(\theta_z=$const.$))$ is better. Then, we determined max$(\theta_{y,1}(\theta_z=$const.$))$, min$(\theta_{y,2}(\theta_z=$const.$))$ and $\theta_{A,max}/$max$(\theta_{y,1}(\theta_z=$const.$))$ as the evaluation indices.
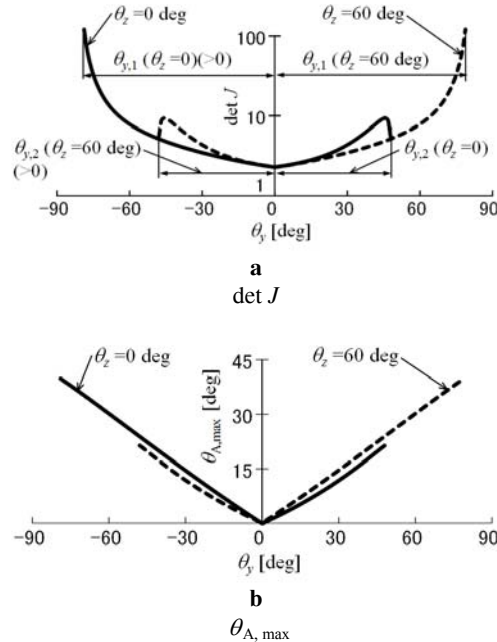

a

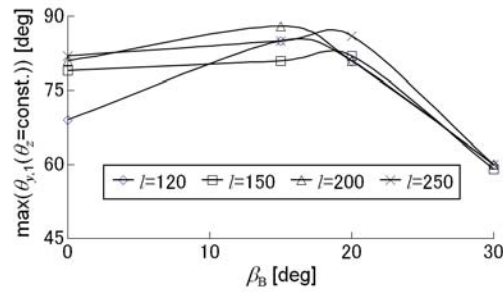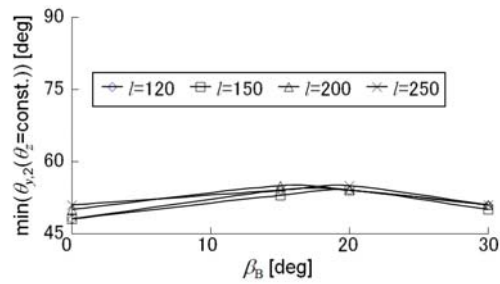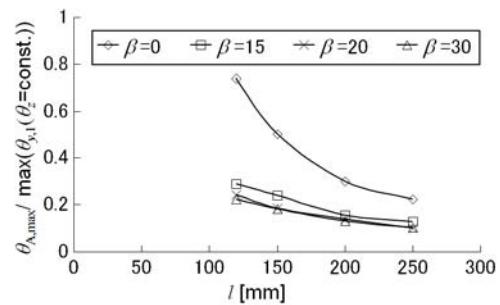det J

b

$\theta_{A,max}$

Fig. 10 – Changes of det J and $\theta_{A,max}$ with respect to θ_y ($r = 45$ mm, $l = 150$ mm, $\beta_B = 0$ deg).

a

$\max(\theta_{y,1}(\theta_z=\text{const.}))$

b

$\min(\theta_{y,2}(\theta_z=\text{const.}))$

c

$\theta_{A,\max}/\max(\theta_{y,1}(\theta_z=\text{const.}))$

Fig. 11 – Relationships between design parameters and evaluation indices (kinematic constants that are not specified are $r = 45$ mm, $l = 150$ mm, $\beta_B = 15$ deg).

4.2. RESULTS

Relationships between the design parameters and the evaluation indices are shown in Fig. 11. It is known from the results that β_B is the most important design
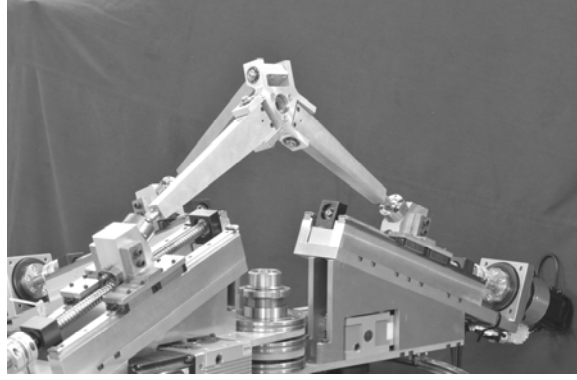
Fig. 12 – A photo of prototype at a pose with a large inclination angle $\theta_y = 80$ deg.

parameter among the kinematic constants for the design of a mechanism that can achieve a high orientation capability and reduce requirement to the motion range of the spherical joint. It is also known that the design parameters have less effect on $\min(\theta_{y,2}(\theta_z=\text{const.}))$ than $\max(\theta_{y,1}(\theta_z=\text{const.}))$.

Based on the analysis results, we optimized the kinematic constants as $r=45$ mm, $l=260$ mm, $\beta_B=20$ deg, then we designed a mechanism. Based on the design, we built a prototype. Its details are described in Section 6. Figure 12 shows a pose with a large inclination angle $\theta_y=80$ deg achieved by the prototype.

5. EVALUATION OF COMPLIANCE AND ACCURACY OF DESIGNED MECHANISM

5.1. EVALUATION INDICES

Figure 13 shows the contact point Q_B of the movable die attached on the output link with the bent pipe and the force $\boldsymbol{f}_B^P$ applied to the movable die from the bent pipe when the pipe is being bent to a circular shape by inclining the movable die by θ_y in the direction of θ_z. Force and moment written at P with respect to the frame P-*xyz* are described as $\boldsymbol{f}_{B,P}^P$ and $\boldsymbol{m}_{B,P}^P$, respectively. Their representations with respect to the frame P-*XYZ* are described as $\boldsymbol{F}_{B,P}$ and $\boldsymbol{M}_{B,P}$, respectively. Coordinates of P_B and Q_B in P-*xyz* are $\boldsymbol{p}_B^P = [0 \quad 0 \quad z_{PB}]^T$ and $\boldsymbol{q}_B^P = [-D\cos\theta_z/2 \quad -D\sin\theta_z/2 \quad 0]^T$, respectively. D is the diameter of the hole of the movable die, which is identical to the outer diameter of the pipe. For simplicity, friction at the contact point is neglected.

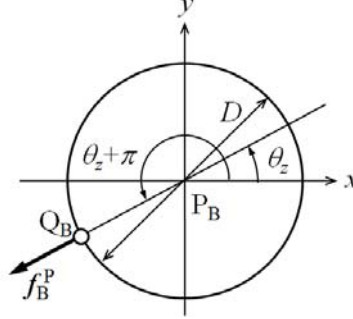Force $\boldsymbol{f}_B^P$ is written as

Fig. 13 – Force applied to the movable die for bending a circular shaped pipe.

$$\boldsymbol{f}_{\mathrm{B}}^{\mathrm{P}} = F_{\mathrm{B}}\boldsymbol{e}_{\mathrm{B}}^{\mathrm{P}}, \tag{15}$$

where F_{B} is the magnitude of the force and $\boldsymbol{e}_{\mathrm{B}}^{\mathrm{P}} = [-\cos\theta_z \quad -\sin\theta_z \quad 0]^{\mathrm{T}}$. $\boldsymbol{f}_{\mathrm{B,P}}^{\mathrm{P}}$ and $\boldsymbol{m}_{\mathrm{B,P}}^{\mathrm{P}}$ are written as

$$\boldsymbol{f}_{\mathrm{B,P}}^{\mathrm{P}} = \boldsymbol{f}_{\mathrm{B}}^{\mathrm{P}}, \quad \boldsymbol{m}_{\mathrm{B,P}}^{\mathrm{P}} = \boldsymbol{p}_{\mathrm{B}}^{\mathrm{P}} \times \boldsymbol{f}_{\mathrm{B}}^{\mathrm{P}} = \begin{bmatrix} z_{\mathrm{PB}}F_{\mathrm{B}}\sin\theta_z \\ -z_{\mathrm{PB}}F_{\mathrm{B}}\cos\theta_z \\ 0 \end{bmatrix}. \tag{16}$$

$\boldsymbol{F}_{\mathrm{B,P}}$ and $\boldsymbol{M}_{\mathrm{B,P}}$ are written as

$$\begin{bmatrix} \boldsymbol{F}_{\mathrm{B,P}} \\ \boldsymbol{M}_{\mathrm{B,P}} \end{bmatrix} = \begin{bmatrix} R_{\mathrm{P}} & 0_3 \\ 0_3 & R_{\mathrm{P}} \end{bmatrix} \begin{bmatrix} \boldsymbol{f}_{\mathrm{B,P}}^{\mathrm{P}} \\ \boldsymbol{m}_{\mathrm{B,P}}^{\mathrm{P}} \end{bmatrix}, \tag{17}$$

where R_{P} is the rotation matrix between the output link coordinate frame and the fixed coordinate frame. From Eq. (13), displacement of P, $\varDelta\boldsymbol{P}_{\mathrm{B}}$, and the angular displacement of the output link, $\varDelta\boldsymbol{\varTheta}_{\mathrm{B}}$, caused by the bending force are represented by using the total compliance C_{MT} as

$$\begin{bmatrix} \varDelta\boldsymbol{P}_{\mathrm{B}} \\ \varDelta\boldsymbol{\varTheta}_{\mathrm{B}} \end{bmatrix} = C_{\mathrm{MT}} \begin{bmatrix} \boldsymbol{F}_{\mathrm{B,P}} \\ \boldsymbol{M}_{\mathrm{B,P}} \end{bmatrix}. \tag{18}$$

The displacement of Q_B, $\varDelta\boldsymbol{Q}_{\mathrm{B}}$, is obtained as

$$\varDelta\boldsymbol{Q}_{\mathrm{B}} = \varDelta\boldsymbol{P}_{\mathrm{B}} + \varDelta\boldsymbol{\varTheta}_{\mathrm{B}} \times \left(R_{\mathrm{P}}\boldsymbol{q}_{\mathrm{B}}^{\mathrm{P}}\right). \tag{19}$$

Then, the displacement of Q_B with respect to P-xyz is obtained as

$$\varDelta\boldsymbol{q}_{\mathrm{B}}^{\mathrm{P}} = R_{\mathrm{P}}^{\mathrm{T}} \varDelta\boldsymbol{Q}_{\mathrm{B}}. \tag{20}$$

The displacement of Q_B in the direction of the force $\boldsymbol{f}_\mathrm{B}^\mathrm{P}$ is obtained as

$$\Delta q_\mathrm{B} = \Delta \boldsymbol{q}_\mathrm{B}^\mathrm{P} \cdot \boldsymbol{e}_\mathrm{B}^\mathrm{P} . \tag{21}$$

Therefore, the compliance of the mechanism at the contact point Q_B is derived as

$$C_\mathrm{M} = \Delta q_\mathrm{B} / F_\mathrm{B} . \tag{22}$$

On the other hand, let us assume that the magnitude of the moment M required for bending a pipe into the same curvature radius R is the same even if the angle θ in Fig. 3a is different. Under this assumption, the ratio of magnitude of the required force F_B for an angle θ to the case of $\theta = 90$ deg becomes $1/\sin\theta$. Then, the magnitude of position error of the contact point Q_B for bending pipes with the same curvature radius is proportional to $C_\mathrm{M}/\sin\theta$. In addition to this, when considering the curvature radius error, this error is magnified by $\pi/(2\theta)$.

Based on the discussions above, the following value is considered as an evaluation index to represent the curvature radius error caused by the compliance of the movable-die drive mechanism:

$$\Delta R_\mathrm{M} = \frac{\pi C_\mathrm{M}}{2\theta \sin\theta} . \tag{23}$$

5.2. RESULTS

Compliance and bending accuracy of the mechanism designed in Section 4.2 (Mech. A: r=45 mm, l=260 mm, β_B=20 deg, z_PB=0 mm, Z_D=40 mm) were evaluated based on the indices C_M and ΔR_M defined in the previous subsection. The mechanism previously used as the movable-die drive mechanism [16] (Mech. B: r=60 mm, l=200 mm, β_B=15 deg, z_PB=25 mm, Z_D=45 mm) was also evaluated for comparison. Considering the cross section (average width = 32 mm, thickness = 20 mm) and material of the link, the feedback gain, the gear ratio of the reduction gear (1/100) and the lead and dimensions of the ball screw used in the prototype, stiffness coefficients of these mechanisms were given as

$$k_\mathrm{L1}=1.6\times10^5 \text{ N/mm} ,$$

$$k_\mathrm{L2}=5.4\times10^2 \text{ N/mm} ,$$

$$k_\mathrm{S1} = 3.6\times10^7 \text{ N}\cdot\text{mm/rad} ,$$

$$k_\mathrm{S2} = 1.0\times10^4 \text{ N/mm} .$$

Figures 14–16 show the results. Calculation was done at 1 deg inclement in θ_y until singular configuration was detected.
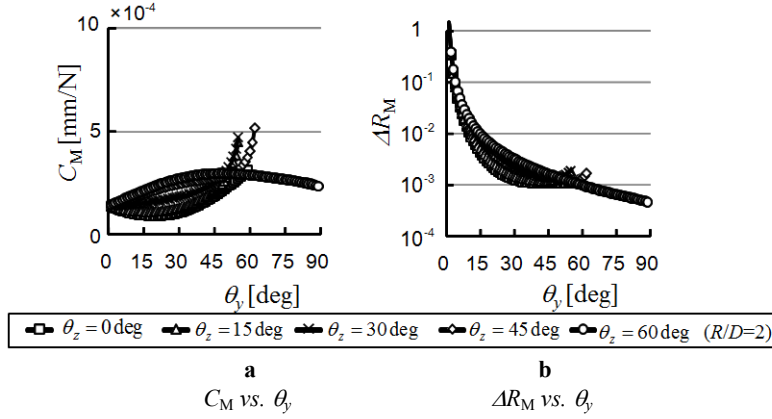
Fig. 14 – C_M and ΔR_M of Mech. A for $R/D = 2$.

Figure 14 shows the relationships between C_M and θ_y and between ΔR_M and θ_y for various θ_z at a constant $R/D = 2$ in Mech. A. It is known from the figure that the curves of $\Delta R_M(\theta_y)$ are almost the same with different values of θ_z though the curves of $C_M(\theta_y)$ change according to the value of θ_z. It is known from Fig. 14a that the compliance C_M is kept within a relatively small range compared with the compliances of the links in a wide range of θ_y. It is also known from Fig. 14b that the curvature radius error ΔR_M gradually reduces according to the increase of θ_y while the mechanism is approaching singular configurations. Similar trends were obtained for different values of $R/D = 4, 6, 8, 10$.

Results of calculation of C_M and ΔR_M for Mech. A and Mech. B at various $R/D = 2, …, 10$ while keeping $\theta_z = 60$ deg are shown in Figs. 15 and 16. These results are summarized as follows:

Compliance C_M

(1) Compliance characteristics of Mech. A are stable in a wide range of θ_y (from 1 deg to the maximum value) for all conditions of R/D though compliance becomes a little bit large around $\theta_y = 45 - 70$ deg when mechanism is located closely to singular configurations. On the other hand, compliance of Mech. B drastically increases according to the increase of θ_y for all conditions of R/D.

(2) Differences in the value of C_M according to the conditions of R/D for Mech. A are small except for the areas indicated by a circle in Fig. 15a. In this area, the mechanism is close to singular configurations. On the other hand, for
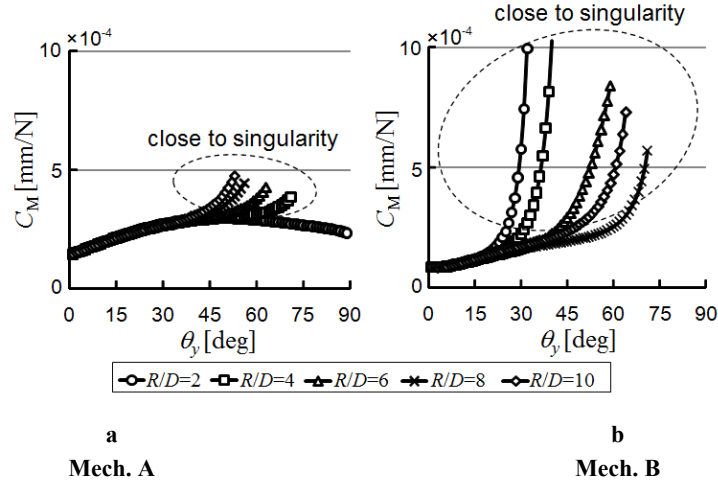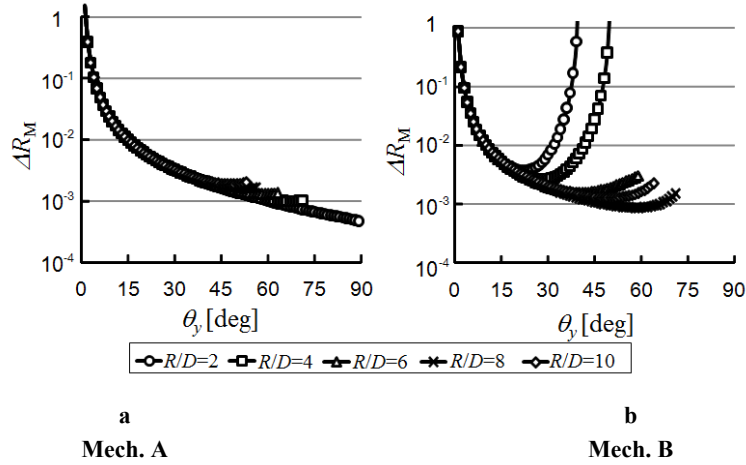
Fig. 15 – Comparison in C_M.

Mech. B, the value of C_M diverges while the mechanism is approaching singular configurations for all R/D by increasing θ_y.

(3) The maximum angle θ_y is dependent on the condition of R/D for both mechanisms. The smaller R/D is, the larger the maximum angle θ_y is in Mech. A. On the other hand, the maximum θ_y is quite dependent on R/D in Mech. B. For the small R/D, the maximum θ_y is small in Mech. B.

(4) Compliance characteristics at $R/D=2$ are quite stable in Mech. A in the whole range of θ_y. This means that there is a wide selection in bending conditions for fabricating pipes with complex shapes. On the other hand, $R/D=8$ is the most selective condition, and $R/D=2$ is the worst in Mech. B.

Curvature radius error ΔR_M

(1) In the range of $\theta_y \leq 15$ deg, both mechanisms have almost the same characteristics in terms of ΔR_M for all conditions of R/D though Mech. B performs a little bit better.

(2) ΔR_M monotonously reduces according to the increase of θ_y for all conditions of R/D in Mech. A though ΔR_M increases a little bit just around the maximum θ_y due to the closeness to singular configurations. This means that the Mech. A performs better in terms of the curvature radius error by selecting

a

Mech. A

b

Mech. B

Fig. 16 – Comparison in ΔR_{M}.

the angle θ_y as large as possible for all R/D. On the other hand, ΔR_{M} drastically increases in Mech. B according to the increase of θ_y for $R/D=2$ and 4 if θ_y exceeds some value (dependent on R/D). As for the conditions of large radius of curvature $R/D \geq 6$, differences in ΔR_{M} between both mechanisms are small.

As discussed above, it is known that the mechanism designed in this paper to improve the orientation capability (Mech. A) performs well in pipe bending by selecting the angle θ_y as large as possible with respect to the fabrication error of bent pipes based on the mechanism compliance characteristics. It is also emphasized that this mechanism performs especially well for fabricating pipes of small curvature radii.

6. PROTOTYPE PIPE BENDER AND EXPERIMENTS

6.1. PROTOTYPE PIPE BENDER

An overview of our prototype pipe bender is shown in Fig. 17a. The configuration of the pipe feeder is shown in Fig. 18. The gripper stage was driven by a servo motor through a ball screw. Since the stroke of the gripper table is 100 mm, the step-by-step motion of the pipe feeder is needed to handle pipes longer than 100 mm. An air cylinder was used as the actuator of the gripper. By

moving the slider A in the downward direction by the air cylinder, the gripper holds the pipe(not shown in the figure). By utilizing the servo effect of the mechanism, the gripping force increases according to the feeding force of the pipe. Therefore, this gripper can tightly hold the pipe with the actuator of small power. The motion of each actuator in the 3-RPSR mechanism and the gripper stage was controlled by a semi-closed-loop controller. A personal computer with the Intel(R) Core(TM) i5-2500 processor (3.3GHz) and a memory (8GB) were used as the controller. The control program was written in C++ language and was executed on MS-Windows 7 (64bit) operating system. The sampling period of controller was 2 ms. As the actuators for the 3-RPSR mechanism and the pipe feeder, we used AC servo motors of rated power 200 W with encoders and reduction gears. As the driving element for the prismatic joint, we used ball screws of a diameter 15 mm and a lead 5 mm. As the spherical joint at A_i, we used the sliding type joint of ball diameter 25.4 mm with a swing angle range ±30 deg manufactured by

a
overview

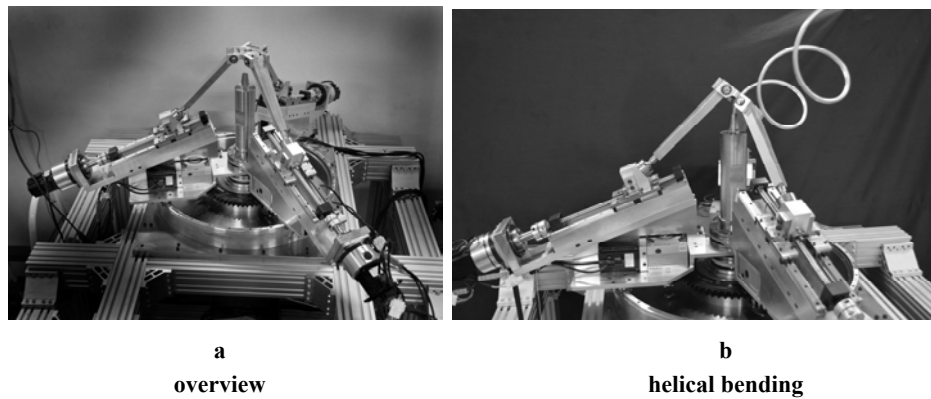**b**
helical bending

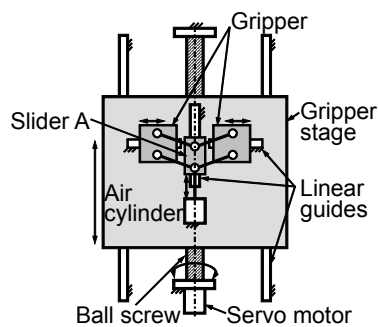Fig. 17 – Prototype pipe bender.

Fig. 18 – Configuration of pipe feeder.

Fig. 19 – Movable die used in experiments.

Hephaist Seiko Co. Ltd. Links were made of duralumin, and shafts were made of steel. The fixed die was made of tool steel with grinding finish, and the movable die was made of nylon (Fig. 19). These dies were designed for pipe of $D = 8$mm.

<div align="center">6.2. EXPERIMENTS</div>

Experimental investigations have been done. We used aluminium pipes of outer diameter $D = 8$ mm with thickness of 1 mm. First, we bent helical pipes using the strategy shown in Fig. 3b. As shown in Fig. 17b, we confirmed that bending a helical pipe can be achieved by our prototype.

Next, we conducted experiments to investigate the effect of the angle θ_y on the accuracy of the bent pipe. Figure 20 shows the photos of the bent pipes of a target radius $R = 50$mm for various conditions in θ_y. The radius of each bent-pipe was measured by taking a photo and fitting a circular curve onto the last one fourth of the entire shape, which is the right-hand side of each pipe shown in Fig. 20 and is the most accurately bent part after initial disturbances having converged. Regarding the measurement, the pixel resolution of images was 0.2 mm and the maximum deviation of the pipe shape against the fitted circle was plus-minus five pixels. Thus, deviation of the real and obtained radii is estimated as at maximum 1 mm. Figure 21 shows the relationship between the ratio of their curvature radius
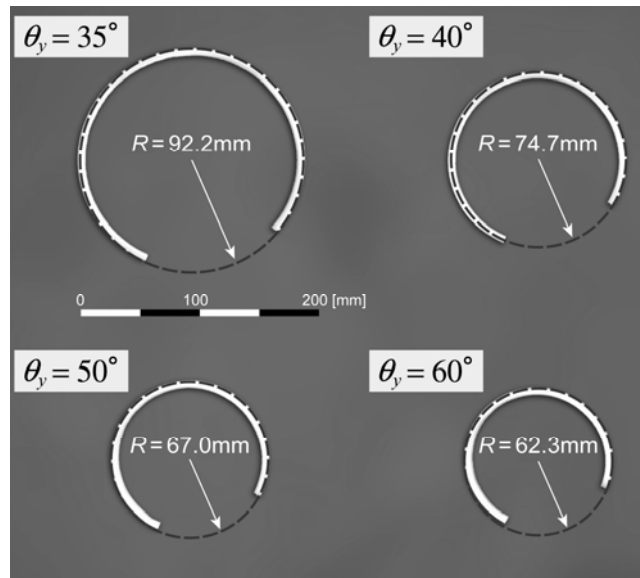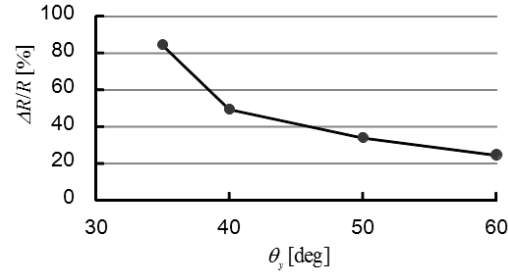

Fig. 20 – Bending results of circular shaped pipes.

Fig. 21 – Curvature radius error obtained by experiments.

errors to R and θ_y. Though we expect that there was a big effect of the clearance between the pipe and fixed and movable dies on the shape accuracy of the bent pipes, it is known from the figure that the angle θ_y has a great effect on the shape accuracy of the bent pipes. That is, accuracy of bending is improved by setting θ_y at an angle as large as possible. This result agrees with the theoretical results shown in the previous section.

7. CONCLUSIONS

Kinematic design of a 3-RPSR parallel mechanism with six DOF, which is intended to apply to the movable-die drive mechanism of a pipe bender, has been done taking into account its orientation capability. Compliance characteristics of the mechanism have been theoretically investigated. Fabrication error of the bent pipes using the mechanism has been measured, and discussed from the point of view of the compliance characteristics of the mechanism. Our conclusions are summarized as follows.

(1) Relationships between the design parameters and orientation capability of the 3-RPSR parallel mechanism have been clarified. Based on the results, a mechanism that can achieve a high orientation capability has been designed.

(2) Evaluation indices for evaluation of compliance characteristics and curvature radius error of the movable-die drive mechanism have been proposed. Based on the indices, effects of the bending conditions, such as the target radius of curvature of bent pipe and the inclination angle of the movable die, on these performances of the designed mechanism have been clarified, and these results have been compared with those of the previous mechanism. As the result, it was clarified that the designed mechanism can have better characteristics, especially for fabricating pipes with small curvature radii.

(3) Experimental results using the prototype pipe bender with the movable-die drive mechanism designed based on the results mentioned above have shown to support the theoretical results.

Future works include motion planning, control and structural design of the movable-die drive mechanism, taking into consideration the geometrical error and the deformation under dynamic condition of the movable-die drive mechanism, the springback effect of the bent pipe and the clearance between the pipe and dies for achieving accurate and fast fabrication of three dimensional complex shaped pipes.

REFERENCES

1. MURATA, M., *Penetration bending method and penetration bending machine therefor*, US patent 5111675, 1992.
2. NEUGEBAUER, R., DROSSEL, W.-G., LORENZ, U., LUETS, N., *Hexabend – A new concept for 3D-free-form bending of tubes and profiles to preform hydroforming parts and endform space-frame-components*, Proceedings of the 7th ICTP, *Advanced Technology of Plasticity*, October 28-31, 2002, Yokohama, Japan, **2**, pp. 1465-1470, 2002.
3. KATAI, H., ICHIRYU, K., *Development of CNC bending machine using 6-axis parallel kinematics mechanism*, Proceedings JSME Annual Meeting 2004, **4**, pp. 75-76, 2004.
4. MURATA, M., KUBOTI, T., TAKAHASHI, K., *Characteristics of tube bending by MOS bending machine*, Proceedings of 2nd International Conference on *New Forming Technology*, Bremen, Germany, pp. 135-144, 2007.
5. FLEHMING, T., HEINEMANN, G., *Auf zukuenftige anforderungen ausgerichtet*, Blech Rohre Profile, **4**, pp. 20-26, 2006.
6. FLEHMING, T., KIBBEN, M., KUEHNI, U., ZIWILER, J., *Device for the free forming and bending longitudinal profiles, particularly pipes, and a combined device for free forming and bending as well as draw bending longitudinal profiles, particularly pipes*, International Patent with application no. PCT/EP2006/00252, 2006.
7. * * *, http://www.tubenet.org/main.shtml
8. GANTNER, P., HARRISON, D.K., DE SILVA, A.K., BAUER, H., *The development of simulation model and the determination of the die control data for the free-bending technique*, Proceedings of Institution of Mechanical Engineers, Part B: Journal of Engineering Manufacture, **221**, pp. 163-171, 2007.
9. NEUGEGAUER, R., PUTS, M., LAUS, G., *The influence of die design on Hexabend technology*, Proceedings of International Conference on *Material Forming* (ESAFORM 2006), April 26-28, 2006, Glasgow, UK, pp. 239-242, 2006.
10. NAOI, H., KITAKAMI, N., MIZUNUMA, M., KURIYAMA, Y., *Study of intrusion bending for steel tubes with thin wall thickness*, Journal of Material Engineering and Performance, **17**, *3*, pp. 376-381, 2008.
11. OTTO-ADAMCZAK, T., HOFFMANN, M., PRIBER, U., *Freiformbiegen mit parallelkinematischer werkzeugfuehrung*, Proceedings of 4th International Conference on *Accuracy in Forming Technology*, ICAFT 2012, November 13-14, 2012, Chemnitz, pp. 465-474, 2012.
12. CORONA, E., *A simple analysis for bend-stretch forming of aluminum extrusions*, International Journal of Mechanical Sciences, **46**, pp. 433-448, 2004.
13. CHATTI, S., HERMES, M., TEKKAYA, A.E., KLEINER, M., *The new TSS bending process: 3D bending of profiles with arbitrary cross-sections*, CIRP Annals – Manufacturing Technology, **59**, pp. 315-318, 2010.

14. TAKEDA, Y., XIAO, X., HIROSE, K., YOSHIDA, Y., ICHIRYU, K., *Kinematic analysis and design of 3-RPSR parallel mechanism with triple revolute joints on the base*, International Journal of Automation Technology, **4**, *1*, pp. 346-354, 2010.
15. TAKEDA, Y., XIAO, X., HIGUCHI, M., INADA, S., HIROSE, K., YOSHIDA, Y., ISHIKURA, Y., *Development of a pipe bender using a parallel mechanism with 3-RPSR structure with six degrees of freedom*, Proceedings of 13th World Congress in *Mechanism and Machine Science*, Guanajuato, Mexico, June 19-25, 2011.
16. TAKEDA, Y., INADA, S., HIGUCHI, M., HIROSE, K., YOSHIDA, Y., ISHIKURA, Y., *Three-dimensional pipe bender using a 3-RPSR parallel mechanism with six degrees of freedom*, Proceedings of the 4th International Conference on *Manufacturing, Machine Design and Tribology*, April 24-27, 2011, Aichi, Japan, pp. 93-94, 2011.
17. TAHMASEBI, F., TSAI, L.W., *Closed-form direct kinematics solution of a new parallel minimanipulator*, Transactions of the ASME, Journal of Mechanical Design, **116**, *4*, pp. 1141-1147, 1994.
18. OIWA, T., *New coordinate measuring machine featuring a parallel mechanism*, International Journal of Japan Society for Precision Engineering, **31**, *3*, pp. 232-233, 1997.
19. KIM, J., PARK, F.C., *Direct kinematic analysis of 3-RS parallel mechanisms*, Mechanism and Machine Theory, **36**, pp. 1121-1134, 2001.
20. NANUA, P., WALDRON, K.J., *Direct kinematic solution of a Stewart platform,* IEEE Transactions on Robotics and Automation, **6**, *4*, pp. 438-444, 1990.
21. BEHI, F., *Kinematic analysis for a six-degree-of-freedom 3-RPRS parallel mechanism*, IEEE Journal of Robotics and Automation, **4**, *5*, pp.561-565, 1998.
22. LEE, K.M., SHAH, D.K., *Kinematic analysis of a three-degrees-of-freedom in-parallel actuated manipulator*, IEEE Journal of Robotics and Automation, **4**, *3*, pp. 354-360, 1988.
23. GOSSELIN, C.M., ANGELES, J., *Singularity analysis of closed-loop kinematic chains*, IEEE Transactions on Robotics and Automation, **6**, *3*, pp. 281-290, 1990.
24. ZLATANOV, D., FENTON, R.G., BENHABIB, B., *A unifying framework for classification and interpretation of mechanism singularities*, Transactions of the ASME, Journal of Mechanical Design, **117**, pp. 566-572, 1995.
25. TAKEDA, Y., *Kinematic analysis of parallel mechanism at singular points where a connecting chain has local mobility*, Mechanism and Machine Theory, **41**, pp. 945-957, 2006.
26. HUNT, K.H., *Kinematic Geometry of Mechanisms*, Clarendon Press, Oxford, 1978.
27. FICHTER, E.F., *A Stewart platform-based manipulator: General theory and practical construction*, The International Journal of Robotics Research, **5**, *2*, pp. 157-182, 1996.
28. FUNABASHI, H., HORIE, M, KUBOTA, T., TAKEDA, Y., *Development of spatial parallel manipulators with six degrees of freedom*, JSME International Journal, Series III, **34**, *3*, pp. 382-387, 1990.
29. MERLET, J.P., *Singular Configurations of parallel manipulators and Grassmann geometry*, The International Journal of Robotics Research, **8**, *5*, pp. 45-56, 1989.
30. TAKEDA, Y., FUNABASHI, H., *Kinematic and static characteristics of in-parallel actuated manipulators at singular points and in their neighborhood*, JSME International Journal, Series C, **39**, *1*, pp. 85-93, 1996.
31. PASHKEVICH, A., KLIMCHIK, A., CHABLAT, D., *Enhanced stiffness modeling of manipulators with passive joints*, Mechanism and Machine Theory, **46**, pp. 662-679, 2011.
32. GOSSELIN, C., *Stiffness mapping for parallel manipulators*, IEEE Transactions on Robotics and Automation, **6**, *3*, pp. 377-382, 1990.
33. GOSSELIN, C.M., ZHANG, D., *Stiffness analysis of parallel mechanism using a lumped model*, International Journal of Robotics and Automation, **17**, pp. 17-27, 2002.
34. WANG Y., LIU, H., HUANG, T., CHETWYND, D.G., *Stiffness modeling of the Tricept robot using the overall Jacobian matrix*, Transactions of the ASME, Journal of Mechanisms and Robotics, **1**, *2*, 021002, 2009.
35. QUENNOUELLE, C., GOSSELIN, C., *Kinetostatic modeling of compliant parallel mechanisms*, Meccanica, **46**, pp. 155-169, 2011.